

Robust Quadruped Jumping via Deep Reinforcement Learning

Guillaume Bellegarda and Quan Nguyen

Abstract—In this paper we consider a general task of jumping varying distances and heights for a quadrupedal robot in noisy environments, such as off of uneven terrain and with variable robot dynamics parameters. To accurately jump in such conditions, we propose a framework using deep reinforcement learning to leverage the complex solution of nonlinear trajectory optimization for quadrupedal jumping. While the standalone optimization limits jumping to take-off from flat ground and requires accurate assumption of robot dynamics, our proposed approach improves the robustness to allow jumping off of significantly uneven terrain with variable robot dynamical parameters. Through our method, the quadruped is able to jump distances of up to 1 m and heights of up to 0.4 m, while being robust to environment noise of foot disturbances of up to 0.1 m in height as well as with 5% variability of its body mass and inertia. This behavior is learned through just a few thousand simulated jumps in PyBullet, and we perform a sim-to-sim transfer to Gazebo. Video results can be found at <https://youtu.be/jkzvL2o3g-s>.

I. INTRODUCTION

Legged robots have potential to accomplish many tasks that may be unsafe for humans, in which overcoming uneven terrain or high obstacles may be necessary. Towards real world deployment, recent works have shown highly dynamic and agile motions such as biped [1] and quadruped [2] back-flips, wheel-legged biped jumping [3], [4], and quadruped running and obstacle jumping [5]. Other quadruped robots showing robust dynamic locomotion include Boston Dynamics’ Big Dog [6], ETH Zurich’s ANYmal [7], IIT’s HyQ [8], and MIT Cheetah 3 [9]. Such methods have used either a simple model for real-time planning, or there is no associated publication.

With respect to optimized jumping, our prior work optimizes over a full planar quadruped model to perform highly dynamic jumps [10]. A tethered quadruped model shows potential for energy efficient lunar jumping with flight phase pitch control through a reaction wheel [11]. Other works have shown single legged [12] and/or dynamic miniature [13], [14] jumping, for which more recent work shows SALTO performing prolonged jumping in non-laboratory settings [15].

To make jumping more robust to external disturbances and new unseen environments, deep learning offers an attractive and generalizable formulation. Deep reinforcement learning in particular has recently shown impressive results in learning control policies for quadrotors [16], [17], bipeds [18], and quadrupeds [19]–[22]. Typically such methods train from

This work is supported by USC Viterbi School of Engineering.

Guillaume Bellegarda and Quan Nguyen are with the Dynamic Robotics and Control Laboratory, Department of Aerospace and Mechanical Engineering, University of Southern California (USC). firstname.lastname@usc.edu

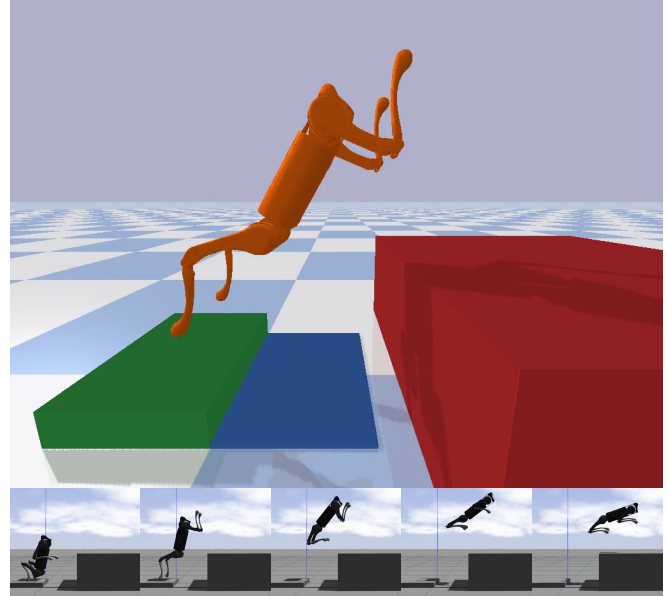


Fig. 1: LASER mini, a mini quadruped robot with leg length of 0.2 m. **Top:** successfully jumping off 0.1 m uneven terrain in PyBullet, with a goal distance of 0.7 m and height 0.4 m. **Bottom:** snapshots from a sim-to-sim transfer to Gazebo.

scratch (i.e. use little or no prior information about the system) and rely on extensive simulation with randomized environment parameters before transferring to hardware.

For legged robots, such methods have largely focused on learning policies in joint space, either through torque control or position control. However, recent works have shown that the choice of action space has a large effect on both training time and policy quality, for general robotic systems ranging from manipulators [23]–[26] to legged systems [27], [28]. These works show that choosing the right action space is critical to learning an optimal policy, and in particular show that selecting actions in Cartesian space with impedance control can outperform learning in joint space, depending on the task. A very recent work shows impressive robustness for real world quadruped deployment in rugged terrain using an even higher level action space, by directly modulating phases for a foot trajectory generator [20].

By contrast, instead of learning jumping motions from scratch in one of these studied action spaces, in this paper we seek to use deep reinforcement learning to improve upon motions produced with a trajectory optimization framework. Under ideal conditions (i.e. starting on flat ground with a high enough coefficient of friction), the motions produced from the optimization can be accurately tracked on hardware,

as shown in [10]. However, under even small disturbances in foot heights (i.e. $< 0.05\text{ m}$), a feedforward controller using only the reference trajectory will lead to taking off at an incorrect pitch angle, causing significant deviation from the desired motion. In addition to the challenges associated with highly dynamic motions, such potential errors come with high risk and can have very costly consequences such as robot damage.

Contribution: We present a method for improving on the performance of the feedforward controller used on optimal trajectories. We learn a general controller to track multiple desired trajectories with deep reinforcement learning, to successfully jump in noisy environments with uneven ground, as shown in Figure 1. This controller is trained on, and able to track, many different jumping trajectories, and works with different joint gains, which can save human trial and error associated with gain tuning. This is particularly relevant as testing joint gains for highly dynamic motions in hardware can be unsafe and/or costly. By learning a single controller capable of achieving many different jumps, this also avoids re-running potentially computationally expensive optimization routines at run time for relatively small differences in initial state. We further validate our method with a sim-to-sim transfer from PyBullet to Gazebo.

The rest of this paper is organized as follows. Section II provides background details on the robot model, reinforcement learning, and gives a brief overview of the jumping trajectory optimization. Section III describes our design choices and training set up for learning to improve the jumping tracking performance. Section IV shows results from learning our general jumping controller, and a brief conclusion is given in Section V.

II. BACKGROUND

A. Robot Model

In this paper, we will validate our jumping controller on the quadruped model LASER (Legged-Agile-Smart-Efficient-Robot). The LASER robot is a highly dynamic quadruped platform built from Unitree’s A1 robot (see Figure 2). The LASER robot has low-inertial legs and high torque density electric motors with planetary gear reduction, and it is capable of ground force control without using any force or torque sensors. The LASER robot uses these high-performance actuators for all the hip, thigh, and knee joints to enable full 3D control of ground reaction forces. It is also equipped with contact sensors on each foot.

The LASER legs feature a large range of motion: the hip joints have a range of motion of $\pm 46^\circ$, the thigh joints have a range of motion from -60° to 240° and the knee joints have a range from -154.5° to -52.5° . The hip and knee designs allow the robot to operate identically forward, backward and flipped upside-down. The robot parameters are summarized in Table I.

Each of LASER’s actuators consists of a custom high torque density electric motor coupled to a single-stage 9:1 planetary gear reduction. The lower link is driven by a bar linkage which passes through the upper link. The legs are

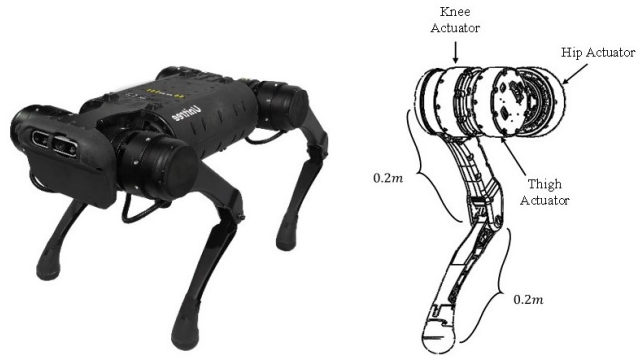


Fig. 2: **Robot Configuration.** Overview of LASER robot and leg configuration

TABLE I: Physical Robot Parameters

Parameter	Symbol	Value	Units
Mass	m	12	kg
Body Inertia	I_{xx}	0.0168	$kg \cdot m^2$
	I_{yy}	0.0565	$kg \cdot m^2$
	I_{zz}	0.0647	$kg \cdot m^2$
Body Length	l_{body}	0.361	m
Body Width	w_{body}	0.194	m
Body Height	h_{body}	0.114	m
Leg Link Lengths	l_1, l_2	0.2	m

TABLE II: Actuator Parameters

Parameter	Value	Units
Gear Ratio	9	
Max Torque	33.5	Nm
Max Joint Speed	21	Rad/s

serially actuated, but to keep leg inertia low, the hip and knee actuators are co-axially located at the hip of each leg. The actuation capabilities of the LASER robot are summarized in Table II.

B. Reinforcement Learning

In the reinforcement learning framework [29], an agent interacts with an environment modeled as a Markov Decision Process (MDP). An MDP is given by a 4-tuple $(\mathcal{S}, \mathcal{A}, \mathcal{P}, \mathcal{R})$, where \mathcal{S} is the set of states, \mathcal{A} is the set of actions available to the agent, $\mathcal{P} : \mathcal{S} \times \mathcal{A} \times \mathcal{S} \rightarrow \mathbb{R}$ is the transition function, where $\mathcal{P}(s_{t+1}|s_t, a_t)$ gives the probability of being in state s_t , taking action a_t , and ending up in state s_{t+1} , and $\mathcal{R} : \mathcal{S} \times \mathcal{A} \times \mathcal{S} \rightarrow \mathbb{R}$ is the reward function, where $\mathcal{R}(s_t, a_t, s_{t+1})$ gives the expected reward for being in state s_t , taking action a_t , and ending up in state s_{t+1} . The goal of an agent is to interact with the environment by selecting actions that will maximize future rewards.

There are several popular algorithms for determining the optimal policy π to maximize the expected return, such as PPO [30], TRPO [31], SAC [32], TD3 [33]. Although we expect any RL algorithm to work in our framework, due to its

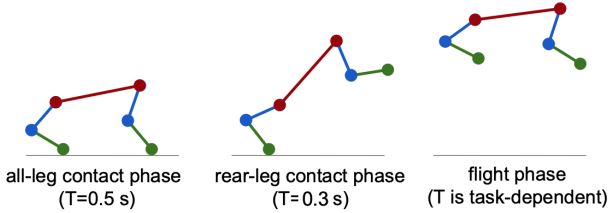


Fig. 3: Jumping motion phases from optimization.

efficiency and stability, in this paper we use Soft-Actor Critic (SAC) [32], which is a state-of-the-art off-policy algorithm for continuous control problems.

SAC learns a policy, $\pi(a|s)$, and a critic, $Q_\phi(s, a)$, and aims to maximize a weighted objective of the reward and the policy entropy, $\mathbb{E}_{s_t, a_t \sim \pi} [\sum_t r_t + \alpha \mathcal{H}(\pi(\cdot|s_t))]$. The critic parameters are learned by minimizing the squared Bellman error using transitions, $\tau_t = (s_t, a_t, s_{t+1}, r_t)$, replayed from an experience buffer, \mathcal{D} :

$$\mathcal{L}_Q(\phi) = \mathbb{E}_{\tau \sim \mathcal{D}} \left[(Q_\phi(s_t, a_t) - (r_t + \gamma V(s_{t+1})))^2 \right] \quad (1)$$

The target value of the next state can be estimated by sampling an action using the current policy:

$$V(s_{t+1}) = \mathbb{E}_{a' \sim \pi} \left[Q_{\tilde{\phi}}(s_{t+1}, a') - \alpha \log \pi(a'|s_{t+1}) \right] \quad (2)$$

where $Q_{\tilde{\phi}}$ represents a more slowly updated copy of the critic. The policy is learned by minimizing the divergence from the exponential of the soft-Q function at the same states:

$$\mathcal{L}_\pi(\psi) = -\mathbb{E}_{a \sim \pi} [Q_\phi(s_t, a) - \alpha \log \pi(a|s_t)] \quad (3)$$

This is done via the reparameterization trick for the newly sampled action, and α is learned against a target entropy.

C. Jumping Trajectory Optimization

In this section we briefly describe the trajectory optimization framework to generate quadruped jumping motions, as well as the associated jumping controller. For full details, please see our prior work [10].

The robot model used in the trajectory optimization framework is a simplified sagittal plane quadruped model consisting of 5 links. The optimization problem is divided into 3 contact phases: double contact (pre-flight preparation), single contact (rear-leg), and flight, as shown in Figure 3. The duration of each phase is manually determined based on desired jumping distance and height.

The resulting discrete time optimization can be formulated as follows:

$$\begin{aligned} & \underset{\mathbf{x}_k, \mathbf{u}_k; k=1 \dots N}{\text{minimize}} && J(\mathbf{x}_N) + h \sum_{k=1}^N w(\mathbf{x}_k, \mathbf{u}_k) \\ & \text{subject to} && d(\mathbf{x}_k, \mathbf{u}_k, \mathbf{x}_{k+1}, \mathbf{u}_{k+1}) = 0, \quad k = 1 \dots N - 1 \\ & && \phi(\mathbf{x}_k, \mathbf{u}_k) = 0, \quad k = 1 \dots N \\ & && \psi(\mathbf{x}_k, \mathbf{u}_k) \geq 0, \quad k = 1 \dots N \end{aligned}$$

where \mathbf{x}_k is the full state of the system at sample k along the trajectory, \mathbf{u}_k is the corresponding control input, J and w are final and additive costs to jump to a particular height and distance while minimizing energy, h is the time between sample points k and $k + 1$, and N is the total number of samples along the trajectory. The function d captures the dynamic constraints, and the functions $\phi(\cdot)$ and $\psi(\cdot)$ capture various constraints on the jumping motions, including joint angle/velocity/torque limits, friction cone limits, minimum ground reaction forces, initial joint and body configurations, pre-landing configuration, final body configuration, and geometric constraints related to the ground and obstacle clearance. Details can be found in [10].

This optimization produces desired joint angles (\mathbf{q}_d), joint velocities ($\dot{\mathbf{q}}_d$) and feed-forward joint torques ($\boldsymbol{\tau}_d$) at a sampling time of 10 ms, which are then linearly interpolated to 1 ms. These can be tracked by the following joint PD controller running at 1 kHz as:

$$\boldsymbol{\tau}_{\text{ff}} = \mathbf{K}_{p, \text{joint}}(\mathbf{q}_d - \mathbf{q}) + \mathbf{K}_{d, \text{joint}}(\dot{\mathbf{q}}_d - \dot{\mathbf{q}}) + \boldsymbol{\tau}_d \quad (4)$$

where $\mathbf{K}_{p, \text{joint}}$ and $\mathbf{K}_{d, \text{joint}}$ are diagonal matrices of proportional and derivative gains in the joint coordinates.

To improve tracking performance, a Cartesian PD controller is added. From the desired joint angle (\mathbf{q}_d) and joint velocity ($\dot{\mathbf{q}}_d$) trajectories, we extract desired foot positions (\mathbf{p}_d) and foot velocities (\mathbf{v}_d) in the leg frame. Thus the full controller for tracking the desired jumping trajectory becomes:

$$\boldsymbol{\tau}_{\text{opt}} = \mathbf{J}(\mathbf{q})^\top [\mathbf{K}_p(\mathbf{p}_d - \mathbf{p}) + \mathbf{K}_d(\mathbf{v}_d - \mathbf{v})] + \boldsymbol{\tau}_{\text{ff}} \quad (5)$$

where $\mathbf{J}(\mathbf{q})$ is the foot Jacobian at joint configuration \mathbf{q} , \mathbf{K}_p and \mathbf{K}_d are diagonal matrices of proportional and derivative gains in Cartesian coordinates, and $\boldsymbol{\tau}_{\text{ff}}$ is the feed-forward torque from Equation 4.

III. IMPROVING JUMPING WITH REINFORCEMENT LEARNING

Given the already established Cartesian and joint space controller for tracking jumping motions, in this section we describe our process and reinforcement learning framework for learning to modify and track these optimal trajectories in the presence of environmental noise and disturbances.

A. Learning Optimal Trajectory Offsets

The choice of action space has been shown to have a significant effect on the learned control policy for robotic systems ranging from manipulators [23]–[25] to legged systems [27], [28], with respect to both training time and policy quality.

In order to provide an intuitive mapping between actions and their effects on the system, we propose learning to appropriately offset the jumping trajectories to cope with disturbances in the environment. Specifically, we consider learning in Cartesian space, with the idea that the agent can more directly observe the effects of its actions, as well as more easily map offsets based on the environment observation, than it can in joint space. In particular, we

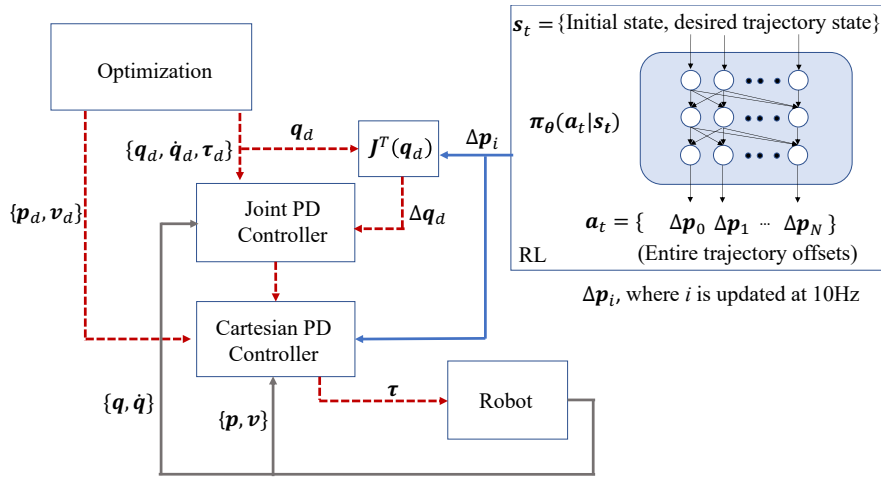


Fig. 4: Control diagram for integrating reinforcement learning action with feedforward jumping controller. The dotted red lines and gray lines execute at 1 kHz , while the blue lines execute at 10 Hz while $t < 0.8\text{ s}$.

consider learning Cartesian space offsets ($\Delta \mathbf{p}_{RL}$) to modify the existing optimal trajectory, which will be combined with the existing jumping controller in Equation 5. The corresponding torque contribution from these Cartesian space offsets can be written as:

$$\boldsymbol{\tau}_{RL\text{ Cartesian}} = \mathbf{J}(\mathbf{q})^\top [\mathbf{K}_p (\Delta \mathbf{p}_{RL} - \mathbf{p})] \quad (6)$$

Such Cartesian space offsets may (attempt to) result in significant deviations in the optimal joint trajectories (\mathbf{q}_d). To avoid joint space gain feedback from counteracting these deviations, we also add offsets in joint space corresponding to those desired in Cartesian space as:

$$\Delta \mathbf{q}_{RL} = \mathbf{J}(\mathbf{q}_d)^\top \Delta \mathbf{p}_{RL} \quad (7)$$

This makes the joint space reinforcement learning torque contribution as follows:

$$\boldsymbol{\tau}_{RL\text{ Joint}} = \mathbf{K}_{p,joint} (\Delta \mathbf{q}_{RL} - \mathbf{q}) \quad (8)$$

The full controller for tracking the desired trajectories with learned reinforcement offsets is then the summation of the original jumping controller (Equation 5) with the offset contributions (Equations 6 and 8):

$$\boldsymbol{\tau} = \boldsymbol{\tau}_{opt} + \boldsymbol{\tau}_{RL\text{ Cartesian}} + \boldsymbol{\tau}_{RL\text{ Joint}} \quad (9)$$

B. Reinforcement Learning Details

There are several challenging aspects of jumping that motivate our observation space, action space, and reward function choices. Firstly, while in the air, it is very difficult to meaningfully adjust body position or orientation. Secondly, even small noise or deviations in the trajectory before take-off can have a large effect on landing location and orientation. Thirdly, the entire motion happens very quickly - with the pre-jump phase taking only 0.8 s , and the flight phase roughly 0.5 s , depending on distance and height.

To mitigate these issues we:

- 1) Learn actions while in contact only, and apply the feedforward controller $\boldsymbol{\tau}_{opt}$ in the air.

- 2) Learn the full trajectory offsets based on the initial conditions as a single state/action, since a disturbance early in the contact phase may make it impossible to recover, and it may not be clear which offsets either caused or contributed to a bad jump. Figure 4 shows the full block diagram for integrating our reinforcement learning action with the feedforward controller, and we describe the MDP below.

Action Space: The action space is thus the desired offsets for the first 0.8 s of the jumping trajectory, and these are all output based on the initial observation. We divide the ground phase into 8 segments of 12 actions each, so the DRL action effectively offsets the trajectory at 10 Hz for 0.8 s .

More concretely, the policy network outputs the full trajectory offset action, $\mathbf{a} \in \mathbb{R}^{12 \times 8 = 96}$, which is then divided into segments and sent as offsets to the jumping controller at 10 Hz . The agent chooses offsets in $[-0.05, 0.05]\text{ m}$ from each foot's local desired (x, y, z) Cartesian positions from the optimization.

Observation Space: The observation space consists of the full robot state at the current initial state, as well as the trajectory end state (goal). More precisely, the initial state consists of: body state (position, orientation, linear and angular velocities), joint state (positions, velocities, torques), foot state (positions, velocities), and foot-in-contact booleans. The trajectory end state contains these same states. The observation space is thus $\mathbf{s} \in \mathbb{R}^{77+77=154}$. These values are first normalized before being used for training purposes by reinforcement learning.

Reward: The reward function attempts to minimize deviations in the body position (x_b, y_b, z_b) and orientation $(\phi_b, \theta_b, \psi_b)$ from the final desired states in the optimal trajectory: body position (x_N, y_N, z_N) and orientation $(\phi_N, \theta_N, \psi_N)$. The final orientation $(\phi_N, \theta_N, \psi_N)$ is always $(0, 0, 0)$ as we consider only planar motions, i.e., the desired landing orientation is always the body x axis. The reward

TABLE III: SAC Hyperparameters.

Parameter	Value
optimizer	Adam
learning rate	$3 \cdot 10^{-4}$
discount (γ)	0.99
replay buffer size	10^6
initial steps	1000
number of hidden layers (all networks)	2
number of hidden units per layer	512
nonlinearity	tanh
batch size	64
target smoothing coefficient (τ)	0.005
target update interval	1
gradient steps	1

function is written as:

$$R(s_t, a_t, s_{t+1}) = w(1 - \|(x_b, y_b, z_b) - (x_N, y_N, z_N)\| - \|(\phi_b, \theta_b, \psi_b)\|) \quad (10)$$

where $w = 100$ is a terminal weight. This reward scheme ensures a reward of w for perfect tracking, and will decrease from there, and even be negative, for very poor tracking.

C. Training Details

We first generate 15 jumping trajectories, with final desired positions ranging in distance in $[0.5, 1.0]$ m and in height in $[0.2, 0.4]$ m . At the beginning of each episode, one of the trajectories is randomly selected to track, and random noise is added to the environment (if applicable). The noise consists of blocks up to 0.1 m in height under each foot, and the body mass and inertia are each varied randomly by up to 5% of their nominal values.

We use PyBullet [34] as the physics engine for training and simulation purposes, and the LASER quadruped model introduced in Sec. II-A. For SAC [32], our neural networks are multi-layer perceptrons with two hidden layers of 512 neurons each, with tanh activation. Other training hyperparameters are listed in Table III.

IV. RESULTS

In this section we discuss results from using our method to improve jumping. Example snapshots of the jumping task are shown in Figures 5 and 6, and the reader is encouraged to watch the supplementary video for clearer visualizations. In particular, we show the results of a sim-to-sim transfer of the learned trajectory-offset policies from PyBullet to Gazebo.

For our experiments, we are specifically interested in the following questions:

1. How does choice of joint gain affect tracking performance?
2. Can we improve upon tracking performance in ideal conditions?
3. How does (magnitude of) noise affect the agent’s ability to learn?

We consider two different sets of joint gains, which we name “high” ($\mathbf{K}_{p,joint} = 300\mathbf{I}_3$, $\mathbf{K}_{d,joint} = 3\mathbf{I}_3$) and “low” ($\mathbf{K}_{p,joint} = 100\mathbf{I}_3$, $\mathbf{K}_{d,joint} = 2\mathbf{I}_3$) gains. Often times these gains must be tuned by hand, and may also need

to be adapted for different trajectories. Thus, our goal with learning with different gains is that it may give some insight on if we can indirectly tune these all at once for multiple trajectories by selecting trajectory offsets, rather than manual human trial and error.

Figure 7 shows training results for learning to offset the trajectories under ideal conditions. With the default baseline “high” joint gain jumping controller, the tracking is already very accurate, getting close to $w = 100$ rewards. On the other hand, the baseline “low” gain controller does not perform as well, primarily due to errors in pitch when at the end of the trajectory, as well as falling short in distance. However, through our framework, we are able to accurately track the desired jumping motions using either set of gains, though the “high” gains still result in slightly better performance. This shows that our framework is general enough to learn to improve several jumping behaviors without the need to explicitly tune gains on a per-motion basis, as may often be needed in general.

Figure 8 shows training results for learning to offset the trajectories under the noisy conditions described in III-C. We train under two sets of noisy environment conditions: with either up to 0.05 m height noise, or up to 0.1 m height noise under each foot, in addition to the variability in body mass and inertia. The baseline controllers for either set of gains are not able to accurately track the desired motions, predominantly due to over/under pitching during the single contact rear back phase. This becomes especially apparent as we increase the environment noise to 0.1 m , where under our reward scheme, the feedforward controller averages approximately 0 reward across 100 random trials, for either set of joint gains, corresponding to extremely poor performance where the robot is not even close to the goal location.

The bottom row of Figure 5 shows the over-pitching behavior of the baseline controller when the front legs start higher than the rear ones, during one of the more difficult jumps in terms of height and distance. This results in jumping vertically and not coming close to landing on the platform.

The bottom of Figure 6 shows the opposite result (under-pitching) when the rear feet start at a higher z height than that of the front feet. In this case, the baseline feedforward controller does not pitch enough before take off, leading to a more horizontal jump that crashes horizontally into the platform. For both of these scenarios, our learned controller is able to successfully jump onto the platform, as can be seen in the top rows of Figures 5 and 6.

A noteworthy observation is that while the “low” gain baseline performance (as well as when training with our method) is not as good as the “high” gain controller for ideal conditions, as the noise increases significantly, we see that the agent is able to exploit the lower gain joint controller to outperform the policy using the high gain controller, as can be seen in Fig. 8.

These results show that through our method, using either set of gains, we are able to learn offsets to significantly improve jumping performance under noisy environmental

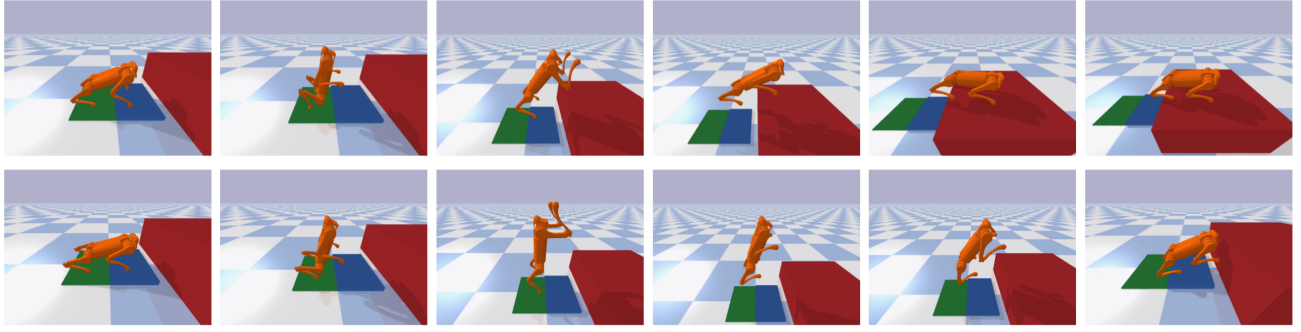


Fig. 5: Motion snapshots of a desired jumping trajectory with distance 0.7 m and height 0.4 m . The front feet have a 0.05 m block beneath them, and the rear feet have a 0.01 m block beneath them. **Top:** The learned policy successfully outputs trajectory offsets to jump onto the platform. **Bottom:** The feedforward controller results in overpitch and overjumps vertically, falling short of the platform.

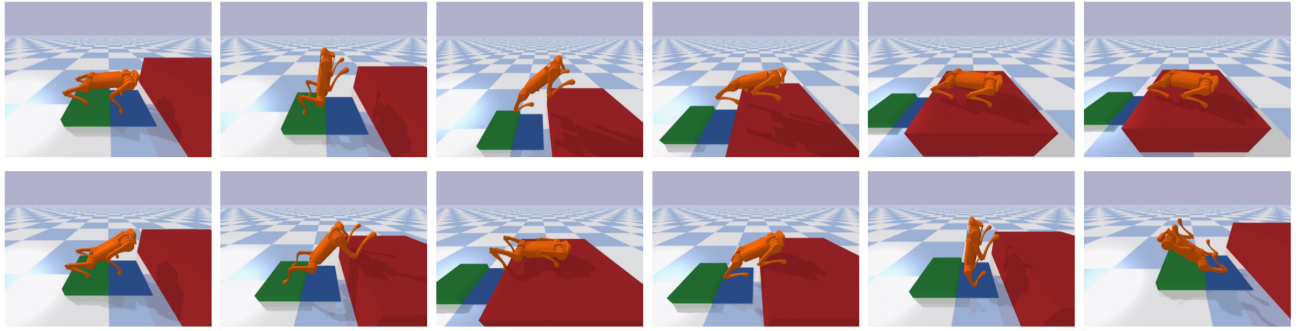


Fig. 6: Motion snapshots of a desired jumping trajectory with distance 0.7 m and height 0.4 m . The front feet have a 0.01 m block beneath them, and the rear feet have a 0.1 m block beneath them. **Top:** The learned policy successfully outputs trajectory offsets to jump onto the platform. **Bottom:** The feedforward controller results in underpitch and overjumps horizontally, making the rear legs catch on the edge of the platform, resulting in falling off.

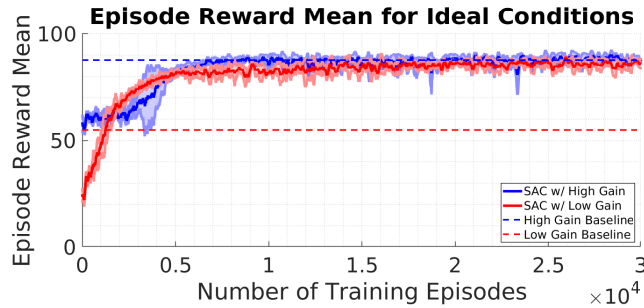


Fig. 7: Episode reward mean while training under ideal conditions. The baseline feedforward controllers’ performance are shown as dotted lines. Our framework is able to track the trajectories accurately for either set of joint gains studied.

conditions, close to as well as under ideal conditions.

V. CONCLUSION

In this work, we proposed a method to improve jumping performance of optimal trajectories with deep reinforcement learning. Instead of learning from scratch, we learn to modify the existing trajectories in Cartesian space, which proved to be robust to significantly varying environmental conditions.

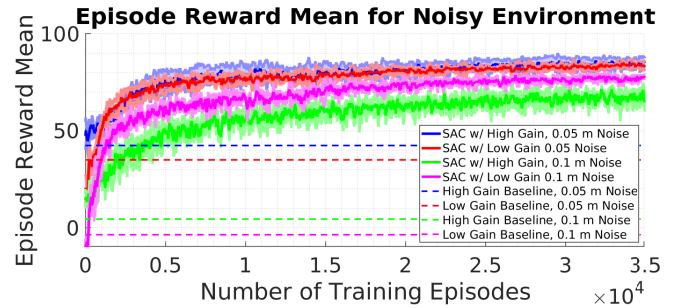


Fig. 8: Episode reward mean while training with noisy environment conditions: either up to 0.05 m or 0.1 m blocks under each foot, and base mass/inertia vary by up to 5% of their nominal values. While the feedforward controllers’ performance is extremely poor, our method is able to learn to jump accurately through significantly noisy environment conditions.

The entire trajectory offsets are learned based on the initial condition and the goal state. In addition to robustness to environmental perturbations, benefits of our method include avoiding manual joint gain tuning, as well as no longer needing to re-run potentially expensive optimization routines

at run time for relatively small changes to the initial robot state, or for uncertainty in the system dynamics.

Due to the success of learning the entire trajectory as one action output, instead of repeatedly querying the policy network as part of the control loop, future work will involve applying this idea to other optimal trajectories and systems. We also plan to expand environmental disturbances to include lateral noise, as well as transfer the jumping framework to hardware to further validate the method.

REFERENCES

- [1] Boston Dynamics. (2017, November) What's new, atlas? [Online]. Available: <https://www.youtube.com/watch?v=fRj34o4hN4I>
- [2] B. Katz, J. Di Carlo, and S. Kim, "Mini cheetah: A platform for pushing the limits of dynamic quadruped control," in *2019 International Conference on Robotics and Automation (ICRA)*. IEEE, 2019, pp. 6295–6301.
- [3] Boston Dynamics. (2017, February) Introducing handle. [Online]. Available: <https://www.youtube.com/watch?v=-7xvqQeoA8c>
- [4] V. Klemm, A. Morra, C. Salzmann, F. Tschopp, K. Bodie, L. Gulich, N. Küng, D. Mannhart, C. Pfister, M. Vierneisel *et al.*, "Ascento: A two-wheeled jumping robot," in *2019 International Conference on Robotics and Automation (ICRA)*. IEEE, 2019, pp. 7515–7521.
- [5] H.-W. Park, P. M. Wensing, and S. Kim, "High-speed bounding with the mit cheetah 2: Control design and experiments," *The International Journal of Robotics Research*, vol. 36, no. 2, pp. 167–192, 2017.
- [6] M. Raibert, K. Blankespoor, G. Nelson, and R. Playter, "Bigdog, the rough-terrain quadruped robot," *IFAC Proceedings Volumes*, vol. 41, no. 2, pp. 10822–10825, 2008.
- [7] M. Hutter, C. Gehring, D. Jud, A. Lauber, C. D. Bellicoso, V. Tsounis, J. Hwangbo, K. Bodie, P. Fankhauser, M. Bloesch *et al.*, "Anymal-a highly mobile and dynamic quadrupedal robot," in *2016 IEEE/RSJ International Conference on Intelligent Robots and Systems (IROS)*. IEEE, 2016, pp. 38–44.
- [8] C. Semini, V. Barasuol, J. Goldsmith, M. Frigerio, M. Focchi, Y. Gao, and D. G. Caldwell, "Design of the hydraulically actuated, torque-controlled quadruped robot hyq2max," *IEEE/ASME Transactions on Mechatronics*, vol. 22, no. 2, pp. 635–646, 2016.
- [9] J. Di Carlo, P. M. Wensing, B. Katz, G. Bledt, and S. Kim, "Dynamic locomotion in the mit cheetah 3 through convex model-predictive control," in *2018 IEEE/RSJ International Conference on Intelligent Robots and Systems (IROS)*, 2018, pp. 1–9.
- [10] Q. Nguyen, M. J. Powell, B. Katz, J. D. Carlo, and S. Kim, "Optimized jumping on the mit cheetah 3 robot," in *2019 International Conference on Robotics and Automation (ICRA)*, 2019, pp. 7448–7454.
- [11] H. Kolvenbach, E. Hampp, P. Barton, R. Zenkl, and M. Hutter, "Towards jumping locomotion for quadruped robots on the moon," in *2019 IEEE/RSJ International Conference on Intelligent Robots and Systems (IROS)*. IEEE, 2019, pp. 5459–5466.
- [12] Y. Ding and H.-W. Park, "Design and experimental implementation of a quasi-direct-drive leg for optimized jumping," in *2017 IEEE/RSJ International Conference on Intelligent Robots and Systems (IROS)*. IEEE, 2017, pp. 300–305.
- [13] D. W. Haldane, M. M. Plecnik, J. K. Yim, and R. S. Fearing, "Robotic vertical jumping agility via series-elastic power modulation," *Science Robotics*, vol. 1, no. 1, 2016.
- [14] M. Noh, S.-W. Kim, S. An, J.-S. Koh, and K.-J. Cho, "Flea-inspired catapult mechanism for miniature jumping robots," *IEEE Transactions on Robotics*, vol. 28, no. 5, pp. 1007–1018, 2012.
- [15] J. K. Yim, E. K. Wang, and R. S. Fearing, "Drift-free roll and pitch estimation for high-acceleration hopping," in *2019 International Conference on Robotics and Automation (ICRA)*. IEEE, 2019, pp. 8986–8992.
- [16] J. Hwangbo, I. Sa, R. Siegwart, and M. Hutter, "Control of a quadrotor with reinforcement learning," *IEEE Robotics and Automation Letters*, vol. 2, no. 4, pp. 2096–2103, 2017.
- [17] A. Molchanov, T. Chen, W. Hönig, J. A. Preiss, N. Ayanian, and G. S. Sukhatme, "Sim-to-(multi)-real: Transfer of low-level robust control policies to multiple quadrotors," in *2019 IEEE/RSJ International Conference on Intelligent Robots and Systems (IROS)*, 2019, pp. 59–66.
- [18] Z. Xie, P. Clary, J. Dao, P. Morais, J. Hurst, and M. van de Panne, "Learning locomotion skills for cassie: Iterative design and sim-to-real," in *Proceedings of the Conference on Robot Learning*, ser. Proceedings of Machine Learning Research, L. P. Kaelbling, D. Kravic, and K. Sugiura, Eds., vol. 100. PMLR, 30 Oct–01 Nov 2020, pp. 317–329.
- [19] J. Hwangbo, J. Lee, A. Dosovitskiy, D. Bellicoso, V. Tsounis, V. Koltun, and M. Hutter, "Learning agile and dynamic motor skills for legged robots," *Science Robotics*, vol. 4, no. 26, 2019.
- [20] J. Lee, J. Hwangbo, L. Wellhausen, V. Koltun, and M. Hutter, "Learning quadrupedal locomotion over challenging terrain," *Science Robotics*, vol. 5, no. 47, 2020. [Online]. Available: <https://robotics.sciencemag.org/content/5/47/eabc5986>
- [21] J. Tan, T. Zhang, E. Coumans, A. Iscen, Y. Bai, D. Hafner, S. Bohez, and V. Vanhoucke, "Sim-to-real: Learning agile locomotion for quadruped robots," in *Proceedings of Robotics: Science and Systems*, Pittsburgh, Pennsylvania, June 2018.
- [22] X. B. Peng, E. Coumans, T. Zhang, T.-W. Lee, J. Tan, and S. Levine, "Learning agile robotic locomotion skills by imitating animals," 2020.
- [23] R. Martín-Martín, M. A. Lee, R. Gardner, S. Savarese, J. Bohg, and A. Garg, "Variable impedance control in end-effector space: An action space for reinforcement learning in contact-rich tasks," in *2019 IEEE/RSJ International Conference on Intelligent Robots and Systems (IROS)*, 2019, pp. 1010–1017.
- [24] F. Stulp, J. Buchli, A. Ellmer, M. Mistry, E. A. Theodorou, and S. Schaal, "Model-free reinforcement learning of impedance control in stochastic environments," *IEEE Transactions on Autonomous Mental Development*, vol. 4, no. 4, pp. 330–341, 2012.
- [25] J. Buchli, E. Theodorou, F. Stulp, and S. Schaal, "Variable impedance control - a reinforcement learning approach," in *Proceedings of Robotics: Science and Systems*, Zaragoza, Spain, June 2010.
- [26] J. Luo, E. Solowjow, C. Wen, J. A. Ojea, A. M. Agogino, A. Tamar, and P. Abbeel, "Reinforcement learning on variable impedance controller for high-precision robotic assembly," in *2019 International Conference on Robotics and Automation (ICRA)*, 2019, pp. 3080–3087.
- [27] X. B. Peng and M. van de Panne, "Learning locomotion skills using deepprl: Does the choice of action space matter?" in *Proceedings of the ACM SIGGRAPH / Eurographics Symposium on Computer Animation*, ser. SCA '17. Association for Computing Machinery, 2017.
- [28] G. Bellegarda and K. Byl, "Training in task space to speed up and guide reinforcement learning," in *2019 IEEE/RSJ International Conference on Intelligent Robots and Systems (IROS)*, 2019, pp. 2693–2699.
- [29] R. S. Sutton and A. G. Barto, *Reinforcement learning - an introduction*, ser. Adaptive computation and machine learning. MIT Press, 1998.
- [30] J. Schulman, F. Wolski, P. Dhariwal, A. Radford, and O. Klimov, "Proximal policy optimization algorithms," *CoRR*, vol. abs/1707.06347, 2017. [Online]. Available: <http://arxiv.org/abs/1707.06347>
- [31] J. Schulman, S. Levine, P. Moritz, M. I. Jordan, and P. Abbeel, "Trust region policy optimization," *CoRR*, vol. abs/1502.05477, 2015. [Online]. Available: <http://arxiv.org/abs/1502.05477>
- [32] T. Haarnoja, A. Zhou, P. Abbeel, and S. Levine, "Soft actor-critic: Off-policy maximum entropy deep reinforcement learning with a stochastic actor," ser. Proceedings of Machine Learning Research, J. Dy and A. Krause, Eds., vol. 80. Stockholmsmässan, Stockholm Sweden: PMLR, 10–15 Jul 2018, pp. 1861–1870. [Online]. Available: <http://proceedings.mlr.press/v80/haarnoja18b.html>
- [33] S. Fujimoto, H. Hoof, and D. Meger, "Addressing function approximation error in actor-critic methods," in *International Conference on Machine Learning*, 2018, pp. 1582–1591.
- [34] E. Coumans and Y. Bai, "Pybullet, a python module for physics simulation for games, robotics and machine learning," <http://pybullet.org>, 2016–2019.